EXPERIMENTAL MEASUREMENT OF THE DYNAMIC PRESSURE DISTRIBUTION IN A SQUEEZE FILM BEARING DAMPER EXECUTING CIRCULAR CENTERED ORBITS

L.A. San Andres and J.M. Vance
Texas A&M University
College Station, Texas 77843

A review of previous experimental measurements of squeeze film damper (SFD) forces is given. Measurements by the authors of SFD pressure fields and force coefficients, for circular centered orbits with $\epsilon = 0.5$, are described and compared with computer predictions. For Reynolds numbers over the range 2-6, the effect of fluid inertia on the pressure fields and forces is found to be significant.

Introduction

Squeeze Film Dampers (SFD) have been the subject of numerous experimental investigations since their development in the early 1960's to attenuate turborotor vibration in aircraft engines. A number of investigators have compared measured pressure fields and/or transmitted forces with predictions based on approximate or limiting geometry solutions to the Reynolds equation for incompressible inertialess flows. Correlation between test and experiments has ranged from good to excellent in some cases to poor in other instances. Among the most important considerations that have been shown to be of considerable influence on the measured pressure profiles and forces are: oil feed mechanisms, use of end seals to prevent axial leakage, level of inlet pressure supply and cavitation pressure of the lubricant, coupling of the damping device to the rotordynamics of the system and, in some circumstances, fluid inertia effects. The review of past experimental work on SFDs treats only the reported investigations for circular centered orbits (CCO). Other types of investigations, although important but less relevant to the subject of the present study, are mainly oriented to determine the overall behavior of rotor systems supported in SFD's.

Thomsen and Anderson [1] studied the range of damping available from the squeeze film by varying the radial clearance and oil viscosity in a test rig. For a centralized preloaded SFD, the damping coefficient was obtained by measuring the deflection in the radial supports of the bearing housing. Comparison with a linearized theory, valid for small amplitude CCO, showed good agreement and independence of the damping coefficient from rotor speed and amplitude of vibration. A significant contribution (although no measured data is presented) is the statement that the measured radial stiffness is much lower than the measured static stiffness, showing the substantial effect of the added mass effect on the oil film forces.

Vance and Kirton [2] carried out an experimental study of the hydrodynamic force response of a damper with end seals. A controlled orbit test rig, independent of the interactions with the rotor bearing systems, was developed. The pressure field was measured around a journal performing circular centered orbits, and then integrated to determine the force components of the squeeze film. Comparisons show fair agreement with the long bearing theory. Paradoxically, larger-than-predicted dimensionless pressures and forces were measured for a light viscocity oil and smaller-than-predicted pressures and forces were measured with high viscosity oil. An attempt to explain the first case was made by suggesting that the damper could be operating in the Taylor Vortex regime. However, the Taylor Vortex regime arises in rotational Couette type flows, and is considered to be a natural convection process resulting from centrifugal forces. The phenomenon would not be expected at all in a SFD. The discrepancy from Reynolds (long bearing) Theory should be attributed to other phenomena, such as oil inlet conditions, which may have caused distortion in the pressure field, or it is possible that the large radial clearance used could have induced significant fluid inertia effects.

Tonnesen [3] obtained damping coefficients by measuring the force impedance of the squeeze film in a test rig for small amplitude centered motions. The measured force coefficients were constant over a considerable speed range provided the transmitted force was below a certain level. As the oil supply was increased, agreement with the full film short SFD theory was found excellent for low frequency motions. With zero supply pressure, the damping capacity of the SFD disappeared and large forces were transmitted to the supports. For offset motions, the correlation was generally poor and misguiding.

Feder, Bansal, and Blanco [4] made an experimental study of a damper with a low L/D ratio (0.3), end seals with negligible leakage, and with oil supplied through small holes in an annular groove at the ends of the damper. A smaller clearance ratio than in reference [2] was used, In this way, the effects of fluid inertia and the lubricant inlet on the squeeze film pressure distribution were minimized. Excellent agreement of measured values with the long bearing theory was reported. Measured pressure profiles and forces were found strongly dependent on the inlet and lubricant cavitation pressures.

Miyachi et. al. [5] conducted measurements of the viscous damping coefficient for a damper with L/D=0.2 and several types of inlet and outlet conditions. The results were compared with numerical predictions from a FEM code. Using simple end plate seals and small inlet holes, as well as a central groove, the measured damping coefficients were much higher than predicted, even in the case of an open ended SFD. For small amplitude motions, and using O-ring and piston ring seals at the ends of the SFD, the measured damping values were consistently higher than predicted, perhaps due to the inherent damping capacity of the end seals. Certainly the end conditions, at the boundaries of the damper are more complicated than the models incorporated in current theories.

Fluid Inertia Studies

The effect of fluid inertia on squeeze film forces has been largely overlooked by rotordynamicists and lubrication engineers, even though theoretical analyses which account for fluid inertia at moderate Reynolds

numbers have predicted large discrepancies from classical lubrication theory. These analyses have raised controversial issues that must be resolved by experimental evidence.

To date, several different measurements of fluid inertial forces in squeeze film configurations have been reported in the literature, but these investigations have mainly been concerned with small amplitude motions of journal about the centered position.

Fritz [6] performed analyses and tests to investigate the added mass and damping forces of a fluid in a thin annulus surrounding a rotor vibrating due to unbalanced forces. Comparison of test and theory gave measured added mass values 25% lower than predicted. The discrepancy was attributed to the axial leakage through the end seals of the test rig. Results also showed the extreme importance of the fluid forces in determining the critical speeds of the rotor.

Chen et. al. [7], and Yang [8] measured the added mass and damping forces for vibrating rods in confined viscous fluids. Results from the damped free oscillations of the rod were compared with numerically predicted results. Correlation of experiment with theory is excellent although the clearance ratios tested were higher than those usually found in lubrication applications.

Mulcahy [9] derived finite length corrections for the fluid forces acting on a central rigid rotor translating periodically in a finite length annular region of confined fluid. Predictions for the added mass are quite satisfactory and within 2.3% of the measured data. Damping showed a variation of 10%, a deviation considered acceptable given the usual scatter encountered in measuring damping values.

There have been some recent efforts directed toward the experimental determination of fluid inertia forces for large amplitude CCOs. In this case the analytical problem becomes more complicated since the full nonlinear Navier-Stokes equations are to be considered. If cavitation is present, a clear isolation of damping and fluid inertia forces is no longer possible. Since damping forces increase rapidly with the orbit radius and are likely to dominate added mass forces, at least for the Reynolds numbers currently found in practice, experimental measurements of fluid inertia forces is more difficult in these operating regions. Tecza et. al. [10] reported experimental results which strongly support the existence of large inertia forces, although inferences must be drawn from the dynamic behavior of the rotor system rather than a direct measurement of damper forces.

Tichy [11] presented measured results which show a substantial effect of fluid inertia in the damping force at quite moderate Reynolds numbers. A tightly sealed damper with an L/D ratio of .15 was used in the experimental work. The journal was constrained to describe CCOs of about 20% and 50% of the radial clearance. Cavitation of the fluid was not allowed. For small Reynolds numbers (<1), the measured film forces were 30% lower than the values from the inertialess solution of the infinitely long bearing theory. These results are opposite to those of Feder [5] referred above. Tichy argues that end leakage is playing an important role in damper behavior.

In Tichy's experiments with Reynolds numbers over the range 2-9, the measured fluid film forces were substantially higher than the values predicted

by the theories which account for fluid inertia effects in the flow. These measured results would be in the right direction if the phase shift between the purely viscous damping and added mass forces increased as the inertial parameter Re increased. However, virtually no change is detected in the phase angle. This striking result means that the total fluid force is always opposite to the journal motion. The added mass effect would thus be almost null.

This paper reports experimental pressure measurements made by the authors to determine the influence of fluid inertia in squeeze film dampers. The test rig employed is a modification of the one used by Vance and Kirton [2]. The modifications were made to improve the accuracy of the measurements and to understand better the test results. The basic concept of the test apparatus is to provide a journal with a known constrained motion within an annular clearance filled with oil, so the characteristics of the squeeze film can be studied independently of the dynamics of the rotor system.

Test Apparatus and Instrumentation

A schematic view of the SFD Test rig is shown in Figure 1. The relevant parameters and basic geometric characteristics of the test rig are given in Appendix 1. The relatively large radial clearance of the squeeze film in the test apparatus is designed to produce significant fluid inertia effects on the film forces at low whirling frequencies.

The journal is mounted on the eccentric lobe of a stiff shaft running on ball bearings with solid steel supports. The shaft is driven through a flexible coupling by an electric motor at a fixed rotational speed of 1770 rpm.

The outer damper bearing housing is supported by bearing index plates using locational fits in order to allow it to rotate through 360 degrees. The journal is prevented from rotation by 4 axial pins, equally spaced, which enter from the end of the journal into a loose fit in the bearing index plates. The ends of the journal are sealed against these plates using O-rings. The axial flow, or amount of leakage, passing the seals is practically zero (none was ever observed).

Oil is supplied to the SFD through a circumferential groove located in the central plane of the bearing housing. The lubricant supply can be varied by using pressurized air and a pressure regulator connected to the supply tank. For the experimental tests reported here, the inlet supply pressure was adjusted to 830 KPa (120 psig) so as to maintain a positive pressure throughout the squeeze film. Cavitation was thereby prevented and a full 360 degree film was developed as shown by the measured pressure waves.

Measurement of the dynamic pressure distribution in the oil film was chosen here over a direct measure of the transmitted forces since the former provides a more direct check of the SFD theories and does not introduce external effects, such as inertia of the housing or forces generated by the end seals. In the axial direction, 3 holes equally spaced 11.11mm(7/16 in) were machined on one side of the central groove. The pressure transducers installed in these holes are designated from end to middle as PT1 to PT3 and correspond, respectively, to the axial distances Z1 to Z3 measured from the closest edge of the groove.

In order to detect if significant changes in the pressure field can be observed at the same axial location but different circumferential position, three holes separated by 120° were tapped at axial location Z2. The measured differences were negligible in preliminary tests with CCO. Thus, as theory indicates, the pressure field around the journal is the same as the dynamic pressure measured at a fixed point for a complete revolution of the shaft and only one pressure transducer is necessary to make the measurement.

Two proximity probes, 90 degrees apart and installed midway between the ends of the bearing, are used to measure the journal center motion and accurately determine the orbit shape and radius. In all the tests performed, it was determined that the orbital motion was circular and centered (CCO) within small tolerances (see Appendix 2).

The pressure transducers are of quartz type and the gap probes are of the eddy-current type. The characteristics of these transducers are given in Appendix 2.

The fluid temperature is measured at the axial location Z2 with a type T thermocouple which is in contact with the lubricant. Oil viscosity is determined from prior measured viscometer data for a range of temperatures, and algebraic expressions are obtained for the fluid viscosity in terms of its temperature using ASTM D-341 formulae.

Two different kinds of oils have been used to date in the experimental procedures: SAE 30 oil (ISO 100) and a silicone fluid (ISO 32). The viscosity versus temperature formula obtained are given in Appendix 2.

Figure 2 shows the instrumentation arrangement. The output voltage of the proximity probe (PP) and the pressure transducers (PT) pass through a signal conditioner calibrated to give a voltage output in the range between +-5 volts. After this operation, the dynamic signals go to an 8 bit analog/digital converter to finally be processed in a desktop computer. At the same time, the oil temperature is read, and the orbit shape and the voltage signal from one of the pressure transducers are displayed and stored in oscilloscopes.

With CCOs and provided the effect of inlet/outlet mechanisms is minimal, the film pressure wave is synchronous with rotor speed and fixed relative to the rotating shaft. Therefore, the measured pressure vs. time waveform could be transformed to a pressure vs. angle relationship. Thus, at the axial location of measurement Zi, experimental fluid film radial and tangential forces and force coefficients are determined by numerical integration of the measured pressure profile for one rotor revolution. Appendix 3 contains the parameters employed to define the dimensionless pressure, p, and film forces and force coefficients at the axial location Zi of measurement.

In the experimental procedure, typically 60 pressure data points were taken for a rotor revolution at the location of measurement, and which corresponds to a data point for every 6° of rotor rotation. This number is considered to describe with detail the film pressure wave and provide calculated film forces with exactitude.

Results and Discussion

Parallel to this experimental investigation, a finite element code was developed to calculate the pressure field, film forces and dynamic force coefficients for finite length SFDs describing circular centered orbits [12]. The analysis, strictly valid for small Reynolds numbers, includes the effect of fluid inertia. Both temporal and convection terms are retained in the nonlinear flow equations which are solved iteratively. Different kinds of inlet and end boundary conditions such as local or global type end seals are included.

The SFD test rig has a length to diameter ratio, L/D, equal to 0.84, a central groove and O-rings at the journal end. Due to these characteristics, neither the long SFD nor short SFD models can be used for comparison with the experimental results.

The following observations, which are relevant to understand the nature of the measured results, were made along the experimentation:

a) Pressure field variations at the same axial location but different circumferential positions were found to be insignificant. This result is a direct consequence of the smallness of the inlet orfice which allowed the pressure waves to be independent of the circumferential location.

b) No oil leakage occured at the damper ends due to the effective sealing action of the O-rings: hence, any through or global axial flow was prevented. Therefore, as measurements confirmed, the region of largest pressures was closer to the damper end walls (at Z1) and decreased as the central groove location was approached.

c) It is a well known practice to assume the pressure is uniform and equal to the supply pressure in a grooved region. However, throughout the experimentation it was found the pressure at the central groove differed considerably from the simple assumption used in practice. Furthermore, the measured pressure gradient in the squeeze film lands was much less than the linear relation expected for a SFD model with uniform pressure at the groove.

By simple geometric similarity and assuming no axial flow and curvature effects, the ratio of pressures in the groove to those in the film lands should be approximately equal to 1/25. However, the observed pressure values at the groove were considerably larger and approximately equal to 1/3 of the film pressure at axial location Z1. These unexpected results can be attributed to the effect of fluid inertia, since at the groove region the Reynolds number is 25 times larger than in the film lands. A Bernoulli type effect and steep pressure gradients are inferred to occur at the interface between the groove and the squeeze film lands.

Thus, the condition of uniform pressure at the inlet of the squeeze film lands was thought to be too simple to be used in the theoretical treatment. The groove acts as a second squeeze film damper and its interface with the squeeze film lands should be provided in terms of flow continuity rather than in pressures due to the Bernoulli type effect most likely to occur in this region. Hence, the groove-squeeze film interface was modelled assuming a local flow constraint was present at the groove edges [13]. This boundary condition

relates the local balance of the axial flow with the pressure drop across the film discontinuity through an End coefficient, $\overline{CL}$, which is a parameter in the flow solution. A value of end coefficient, $\overline{CL}$=0, represents a uniform axial film geometry; while as $\overline{CL}$ approaches ∞, a uniform pressure at the groove is obtained.

This type of ad-hoc procedure has also been used in the experimental work reported in [10]. In it, a damper with inlet and drain grooves was modelled as if it was locally sealed so as to obtain closer agreement between measured and predicted forces.

From a parametric study performed, values of the end coefficient, $\overline{CL}$, in the range from 0.2 to 0.3 were found to predict film pressures which closely matched those at Z1. Then, a value of $\overline{CL}$=0.25 was subsequently selected to predict film forces and compare with the experimental results at axial locations Z1 and Z2.

At this point, a brief explanation of the effect of fluid inertia on the film pressures for the full film solution is thought to be necessary. Consider, as in Figure 3a, a journal contrained to perform circular centered orbits of dimensionless radius e/c and frequency ω. If fluid inertia is neglected in the analysis, Figure 3b shows the predicted dynamic pressure wave p observed at circumferential position A and Z2 as the journal center describes a complete orbit. The purely viscous dynamic pressure is in phase with the film thickness velocity, i.e. is zero when the gap time rate of change is zero (at $\omega t=0,\pi,2\pi$, etc.) The pressure is antisymmetric with respect to the line $\omega t=\pi$ and the same level of peak positive and negative pressures are obtained.

The inclusion of fluid inertia gives rise to an additional pressure field which is in phase with the acceleration of the film thickness H. Figure 3b shows the pressure wave solely due to fluid inertia for increasing values of the squeeze film Reynolds number. Minimum and maximum pressures are given at $\omega t=0$ and π where the gap acceleration has its extreme values. The purely inertial pressure field is symmetric with respect to the line $\omega t=\pi$.

Figure 4 shows the addition of the purely viscous and inertial pressure waves for increasing values of the Reynolds number. The significant effect that fluid inertia has on the film pressures is clearly seen; at the minimum film locations ($\omega t=0,2\pi,4\pi$) the dynamic pressure has a negative value, while at the maximum gap locations the pressure gets above the zero pressure line. For increasing Reynolds numbers, the peak negative pressures p increase in an absolute sense, while the maximum peak positive pressure p stays relatively constant.

Figures 5, 6 and 7 show a comparison between the measured and predicted pressure waves at Z2 for Reynolds numbers equal to 2.54, 4, and 5.137, respectively. The experimental pressure waves show clearly the effect of fluid inertia as outlined above, and the good comparison with the finite element predictions is typical of most measurements. Measured pressures at locations Z1 and Z3 are similar in form to those at Z2, and are not reproduced here for brevity.

Figure 8 shows the peak experimental dynamic pressures p at the axial locations of measurement as the Reynolds number, Re, increases. The

predictions for the SFD model with a $\overline{CL}$=0.25 are also included in the figure, and it is seen the predicted axial pressure drop follows approximately the measured pressure drop.

Fluid film forces and force coefficients at the axial locations of measurement, Zi, are determined by integration of the measured pressure profile for one rotor revolution. Figures 9 and 10 show, as the Reynolds number increases, the direct damping and inertia force coefficients, $\overline{Ctt}$ and $\overline{Drr}$ calculated from the experimental pressure data. The damping coefficients range between 65% to 85% of the damping value for the long SFD model. Comparison with the predictions is regarded as satisfactory considering the limitations of the model employed. The inertia coefficients show a better agreement with the predictions, although discrepancies exist for the largest Reynolds number tested. Figure 10 also includes predicted values of $\overline{Drr}$ for a SFD model which only accounts for temporal inertia terms in the flow model [14]; comparison with the experimental results emphasizes that a large error in inertia force predictions are made if a linearized model is used in damper design.

Figures 11 and 12 show the total dimensionless film force f and the force phase angle obtained from the force coefficients given in Figures 10 and 11. is the angle of the resultant force f and measured from the maximum film thickness. The predictions from the SFD model with $\overline{CL}$=0.25 are in an average sense close to the values calculated from the measured pressures. The effect of fluid inertia in the experimental results is seen to be significant specially in regard to the force phase angle which shows a 20° shift, at the highest Re, when compared to the 90° value derived from lubrication inertialess theories.

Conclusions

The effect of fluid inertia on the pressure field and film forces in a squeeze film damper test rig with circular centered orbits has been measured experimentally for one value of the dimensionless orbit radius (e/c=0.5).

Large levels of pressures were observed at the damper central groove and its influence on the measured pressures in the squeeze film lands is of paramont importance in the damper performance. The groove-squeeze film interface was modelled by assuming a balance between the local axial flow and pressure drop across the interface. An end coefficient, $\overline{CL}$=0.25, was determined to reproduce satisfactorily the measured pressure field.

Comparison of the experimental results with predictions from a non linear finite element SFD model are regarded good considering that fluid inertia renders the problem close to untractable even by numerical means. Major discrepancies are attributed to the limitation of the fluid flow model employed and which is strictly valid for low values of the squeeze film Reynolds number.

Previous analyses of fluid inertia effects on SFDs, which take into account only temporal terms [14], are shown to be in error for prediction of fluid inertia SFD forces.

The experimental measurements have shown that there is an urgent need to develop better theoretical boundary conditions which will account for the local detailed effects of fluid inertia and film geometry.

APPENDIX 1

Components of squeeze film damper test rig. Nominal dimensions and general characteristics.

Angular speed of eccentric shaft:	185.35 rad/sec (1770 rpm)	
	Dimension	
Journal Diameter:	127.000 mm(5.000 in)	
Length :	119.702 mm(4.712 in)	
Bearing Diameter:	130.175 mm(5.125 in)	
Radial clearance:	1.587 mm(1/16 in)	
Orbit radius :	0.794 mm(1/32 in)	
Central groove depth :	6.350 mm(1/4 in)	
width :	12.700 mm(1/2 in)	
Inlet orifice : Diameter:	0.400 mm(1/64 in)	
Axial distance from edge of central groove to pressure transducers		Z/R
to PT1 (Z1):	42.773 mm(1.684 in)	0.657
to PT2 (Z2):	31.554 mm(1.242 in)	0.485
to PT3 (Z3):	20.570 mm(0.810 in)	0.3157

Dimensionless orbit radius: $\varepsilon = e/c = 0.50$
Dimensionless clearance ratio: $\delta = c/R = 0.025$
Damper test rig L/D ratio: 0.8425

Note: For parameter L/D, groove width has not been considered in calculation.

APPENDIX 2

1. Characteristics of quartz pressure transducers:

Average sensitivity: 0.7251 mv/KPa (4.99 mv/psi)
Linearity: 0.2% of full scale
Range: 0 - 6895 KPa (0 - 1000 psi)

2. Characteristics of proximity system:

Scale factor: 7.865 V/mm (200 mv/mil) + 0.4%
Linearity: 0.15% of full scale
Range: 1.143 - 3.81 mm (45 - 150 mils)

3. Oil viscosity formulae and range of viscosities and squeeze film Reynolds numbers tested:

viscosity ν in centistokes:

$$\log[\log(\nu+0.7)] = a + b \log[1.8\ T(^{\circ}C) + 492]$$

Factor	SAE 30 oil	Silicone fluid
a	10.052320	3.87822
b	-3.542052	-1.31010
r*	0.997500	0.99530
Specific gravity at 21°C(70°F)	0.8710	0.960
Range of tested oil temperatures	25 - 44 °C	25 - 37 °C
Range of measured oil viscosities	226 - 85 cst	100 - 79 cst
Range of tested Reynolds numbers	2 - 5.50	4.7 - 5.9

r*: denotes the correlation of linear regression analysis of experimental data.

4. Dimensional tolerances of the test rig and its orbital motion for circular centered orbits.

Radial clearance (c): 1.618 mm(0.0637 in) maximum
1.584 mm(0.0624 in) minimum

Dimensiolness orbit radius (e/c): 0.51072 maximum
0.48972 minimum

Dimensionless journal center offsets: $\delta x/c = 1.223 \times 10^{-5}$
$\delta y/c = 615.521 \times 10^{-5}$

APPENDIX 3

Definition of dimensionless pressure and force coefficients at axial locations of measurement

Squeeze film Reynolds number: $Re = \omega \cdot c / \nu$

Dimensionless pressure: $\bar{p}(\theta, z) = p/Cp; \quad Cp = \mu w R^2/c^2$

Radial and tangential dimensionless fluid film forces:

$$fr = Fr/Cf = \int_0^1 \oint \bar{p} \cdot \cos\theta \, d\theta \, d\beta = \sum_{i=1}^{N} fr_i \, \Delta\beta$$

$$ft = Ft/Cf = \int \oint \bar{p} \cdot \sin\theta \, d\theta \, d\beta = \sum_{i=1}^{N} ft_i \, \Delta\beta$$

$\beta = z/L$, $Cf = \mu \omega L R^3/c^2$, N: N° of axial locations of measurement

fr_i and ft_i are local dimensionless film forces at Z_i, the axial location of measurement, and given by:

$$fr_i = 0 \, \bar{p}(\theta, \beta_i) \cdot \cos\theta \, d\theta; \quad ft_i = 0 \, \bar{p}(\theta, \beta_i) \cdot \sin\theta \, d\theta$$

Total film force: $f_i = [(fr_i)^2 + (ft_i)]^{2\,1/2}$

Force phase angle: $\phi_i + 90^\circ + tg^{-1}(fr_i/ft_i)$ measured from maximum gap location

Local damping, $\overline{Ctt}_i$, and inertia, $\overline{Drr}_1$, force coefficients at the axial location Z_i of measurement are defined as:

$$\overline{Ctt}_i = -ft_i/\epsilon \quad ; \quad \overline{Drr}_i = fr_i/\epsilon$$

Global dimensional values of the force coefficients are given approximately by:

$$Ctt = -Ft/(\omega e) = \mu L R^3/C^3 \sum_{i=1}^{N} \overline{Ctt}_i \, \Delta\beta_i$$

$$Drr = -Fr/(-\omega^2 e) = \mu \omega L R^3/c^3 \sum_{i=1}^{N} \overline{Drr}_i \, \Delta\beta_i$$

References

1. Thomesen K.K., and H. Andersen, "Experimental Investigation of a Simple Squeeze Film Damper," Journal of Engineering for Industry, May 1974, pp. 427-430.

2. Vance J.M., and A.J. Kirton, "Experimental Measurement of the Dynamic Force Response of a Squeeze-Film Bearing Damper," Journal of Engineering for Industry, November 1975, pp 1282-1290.

3. Tonnesen J., "Experimental Parametric Study of a Squeeze Film Bearing," Journal of Lubrication Technology, April 1976, pp. 206-212.

4. Feder E., P.N. Bansal, and A. Blanco, "Investigation of Squeeze Film Damper Forces Produced by Circular Centered Orbits," Journal of Engineering for Power, Jan. 1978, v.100, pp. 15-21.

5. Miyachi T., S. Hoshiya, Y. Matsuki, and T. Torisaki, "Oil Squeeze Film Dampers For Reducing Vibration of Aircraft Gas Turbine Engines," ASME paper 79-GT-133, 1979.

6. Fritz, R.J., "The effects of an Annular Fluid on the Vibrations of a Long Rotor, Part 2 - Test," Journal of Basic Engineering, December 1970, pp. 930-937.

7. Chen S.S., M.W. Wambsganss, and J.A. Jendrezejczyk, "Added Mass and Damping of a Vibrating Rod in Confined Viscous Fluids," Journal of Applied Mechanics, June 1976, pp. 325-329.

8. Yang, C.I., and T.J. Moran, "Finite Element Solution of Added Mass and Damping of Oscillation Rods in Viscous Fluids," Journal of Applied Mechanics, September 1979, v. 46, pp. 519-522.

9. Mulcahy T.M., "Fluid Forces on Rods Vibrating in Finite Length Annular Regions," Journal of Applied Mechanics, June 1980, v. 47, pp. 234-240.

10. Tecza, J.A., J.C. Giordano, E.S. Zorzi, and S.K. Drake, "Squeeze-Film Damper Technology: Part 2 - Experimental Verification Using a Controlled-Orbit Test Rig," ASME paper 83-GT-248, 1983.

11. Tichy, J.A., "Measurements of Squeeze Film Bearing Forces to Demonstrate the Effect of Fluid Inertia," ASME paper 84-GT-11, 1984.

12. San Andre's, L.A., "Effect of Fluid Inertia on Squeeze Film Damper Force Response," Ph. D. Dissertation in Mechanical

13. Marmel, R.A., and J.M. Vance, "Squeeze Film Damper Characteristics for Gas Turbine Engines," Journal of Mechanical Design, ASME Trans., Vol. 100, 1978, pp. 139-146.

14. Lund, J.W., A.J. Smalley, J.A. Tecza, and J.F. Walton, "Squeeze Film Damper Technology. Part 1: Prediction of Finite Length Damper Performance," ASME Trans., Paper No. 83-9T-247, 1983.

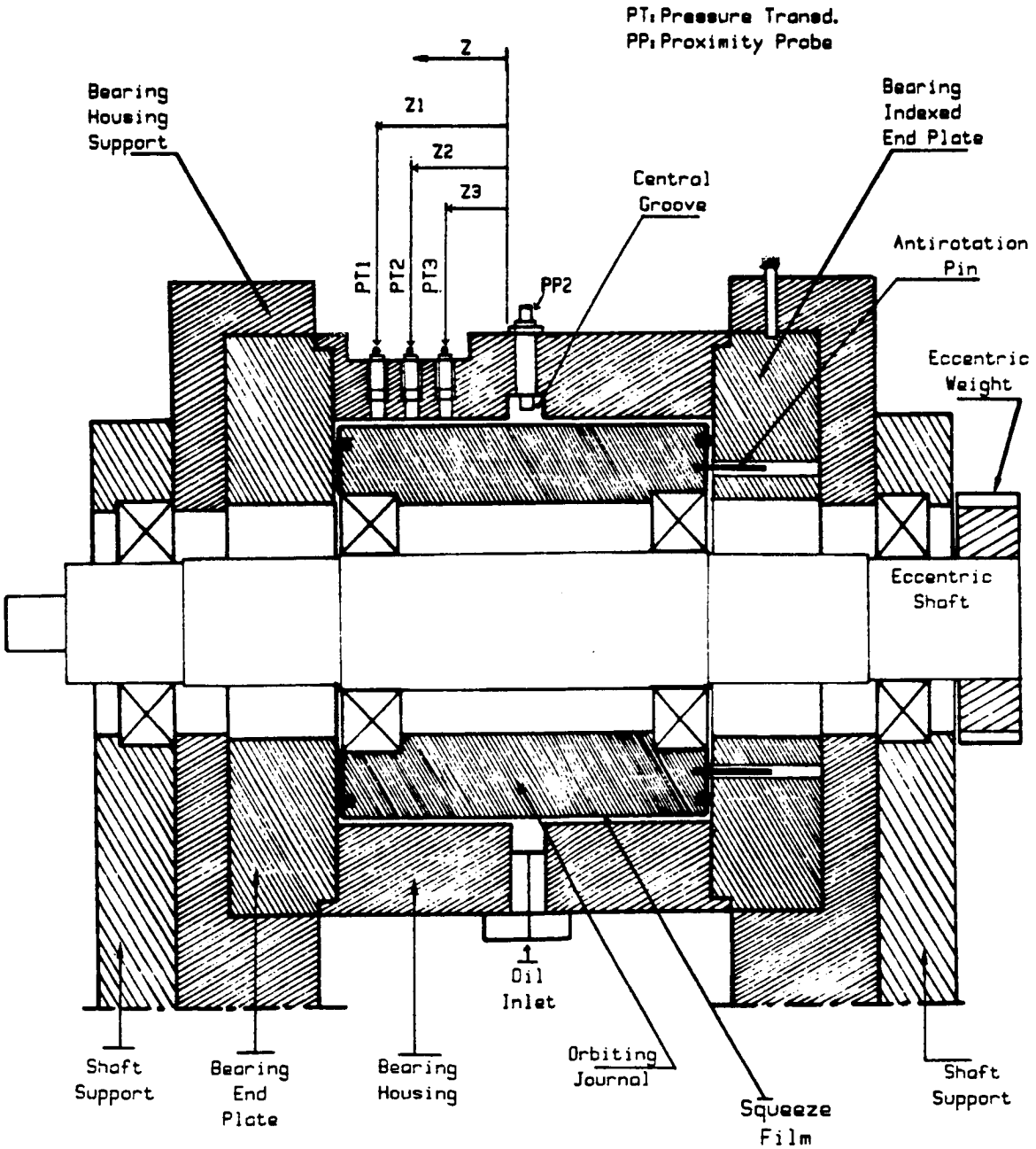

Figure 1. Squeeze Film Damper Test Rig. Axial cross section.

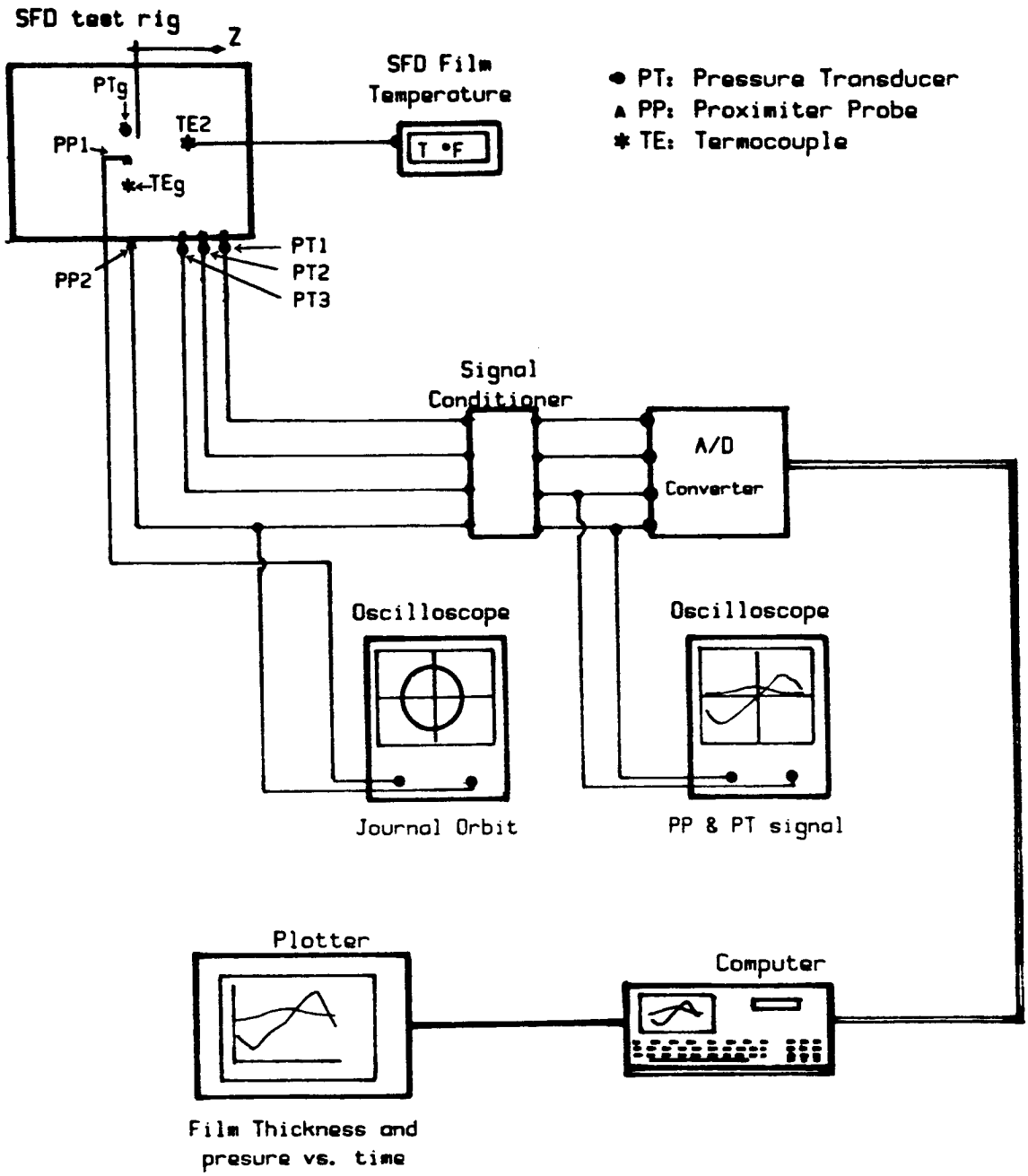

Figure 2. Schematic drawing of Instrumentation for SFD test rig.

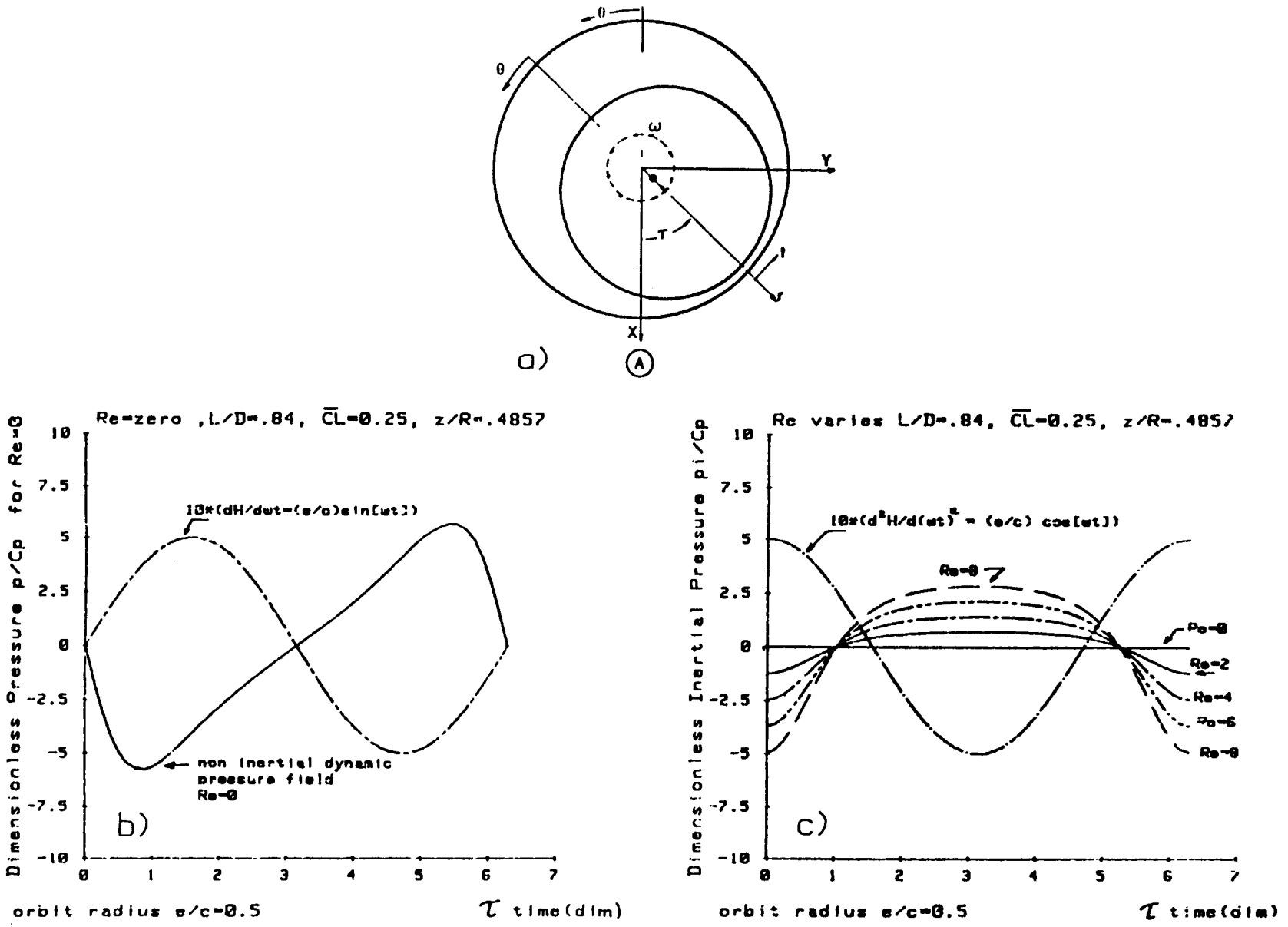

Figure 3. Film thickness H and predicted purely viscous and inertial dimensionless pressures for SFD model: L/D=0.84 and end coefficient CL=0.25, at axial location Z2.

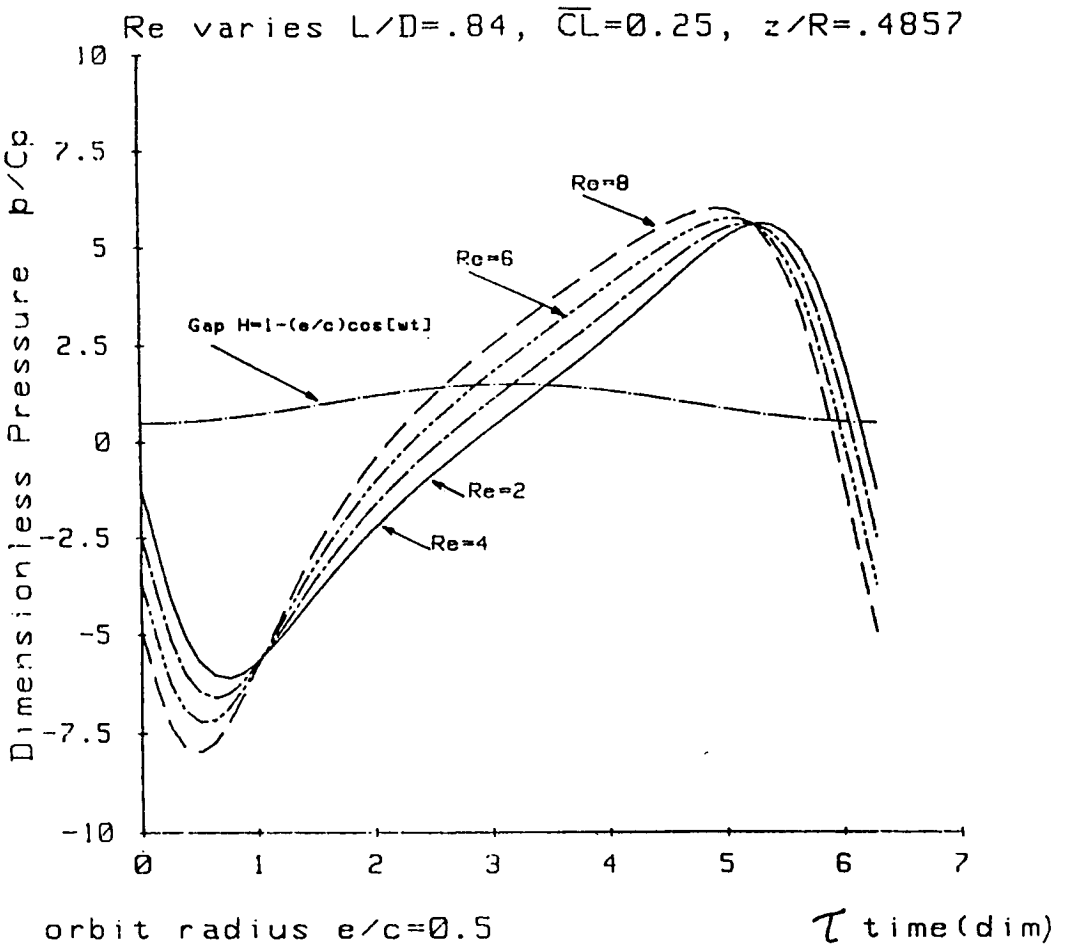

Figure 4. Predicted total dimensionless pressure vs. time for SFD model: L/D=0.84, $\overline{CL}$=0.25, at axial location Z2.

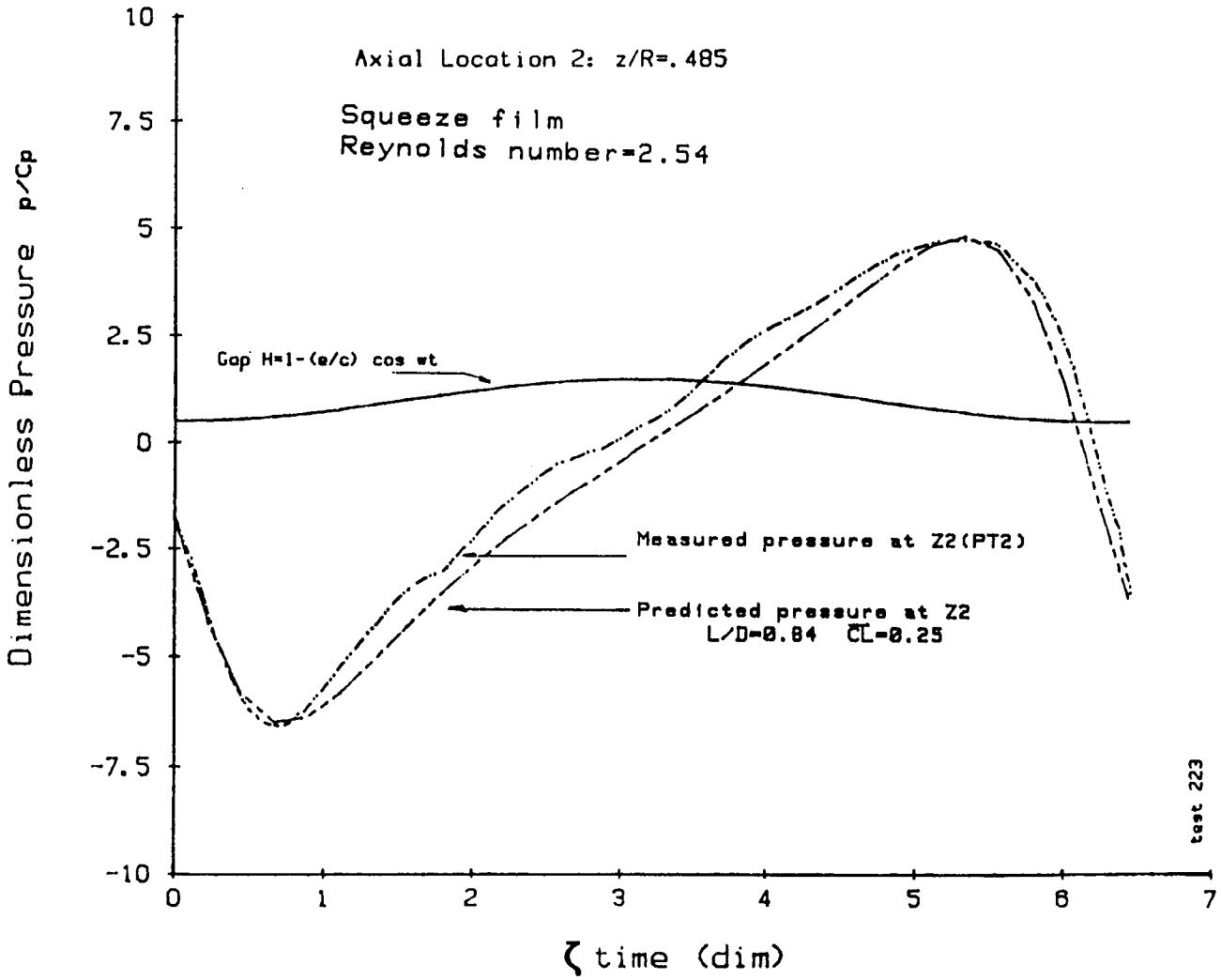

Figure 5. Dimensionless pressure wave $\bar{p}$ vs. wt at axial location Z2. Re=2.54. Experimental and predicted results.

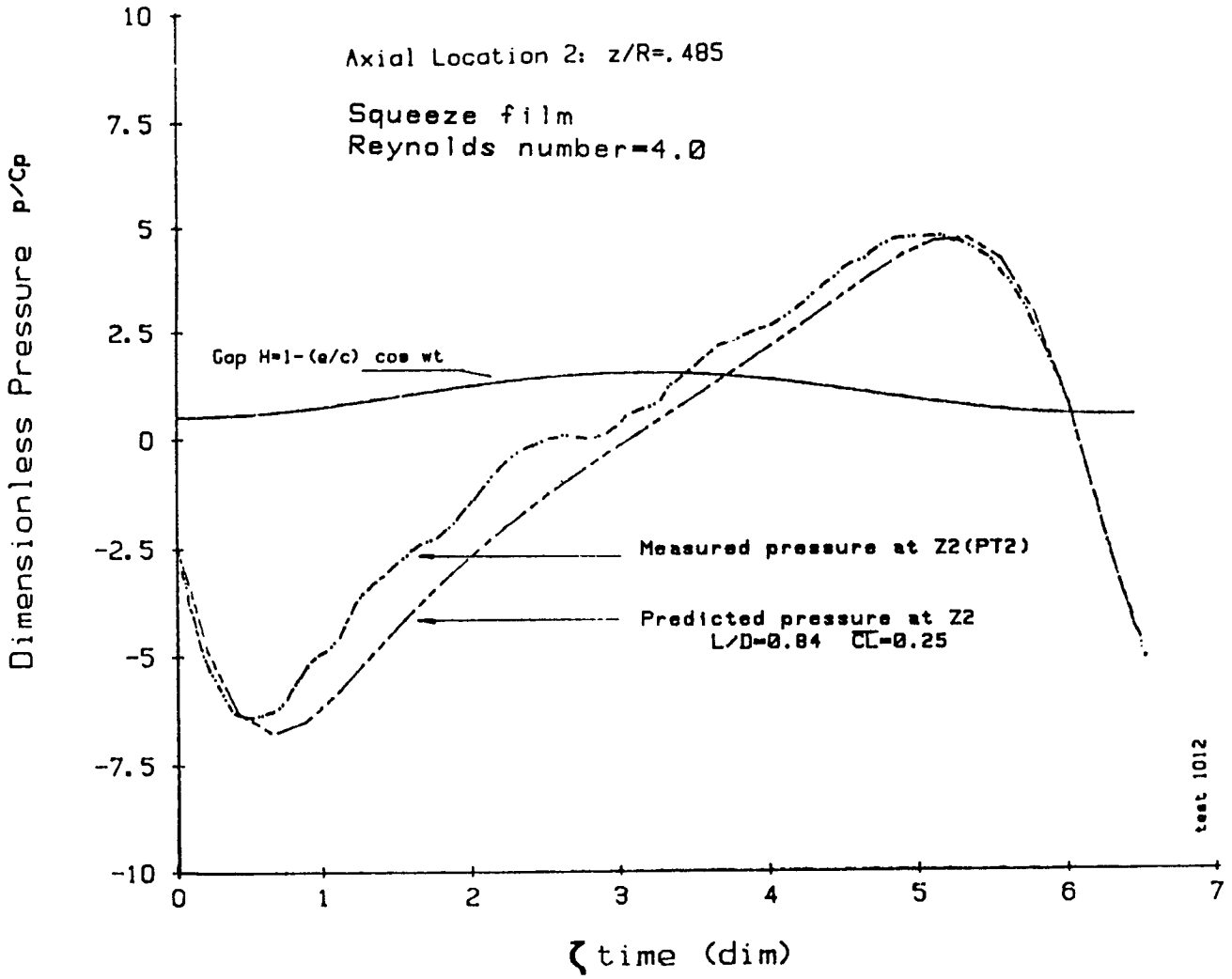

Figure 6. Dimensionless pressure wave $\bar{p}$ vs. wt at axial location Z2. Re=4.00. Experimental and predicted results.

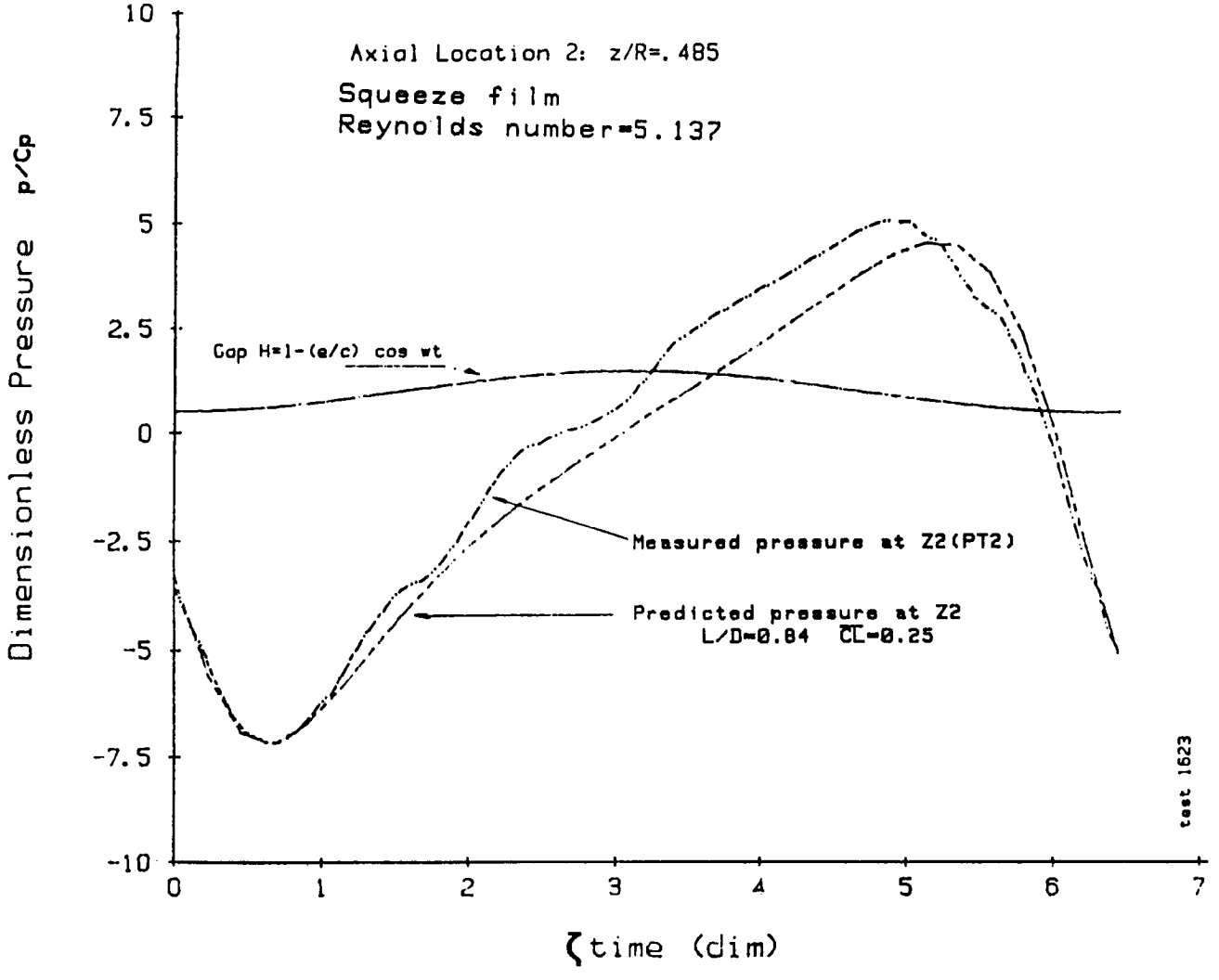

Figure 7. Dimensionless pressure wave $\overline{p}$ vs. wt at axial location Z2. Re=5.137. Experimental and predicted results.

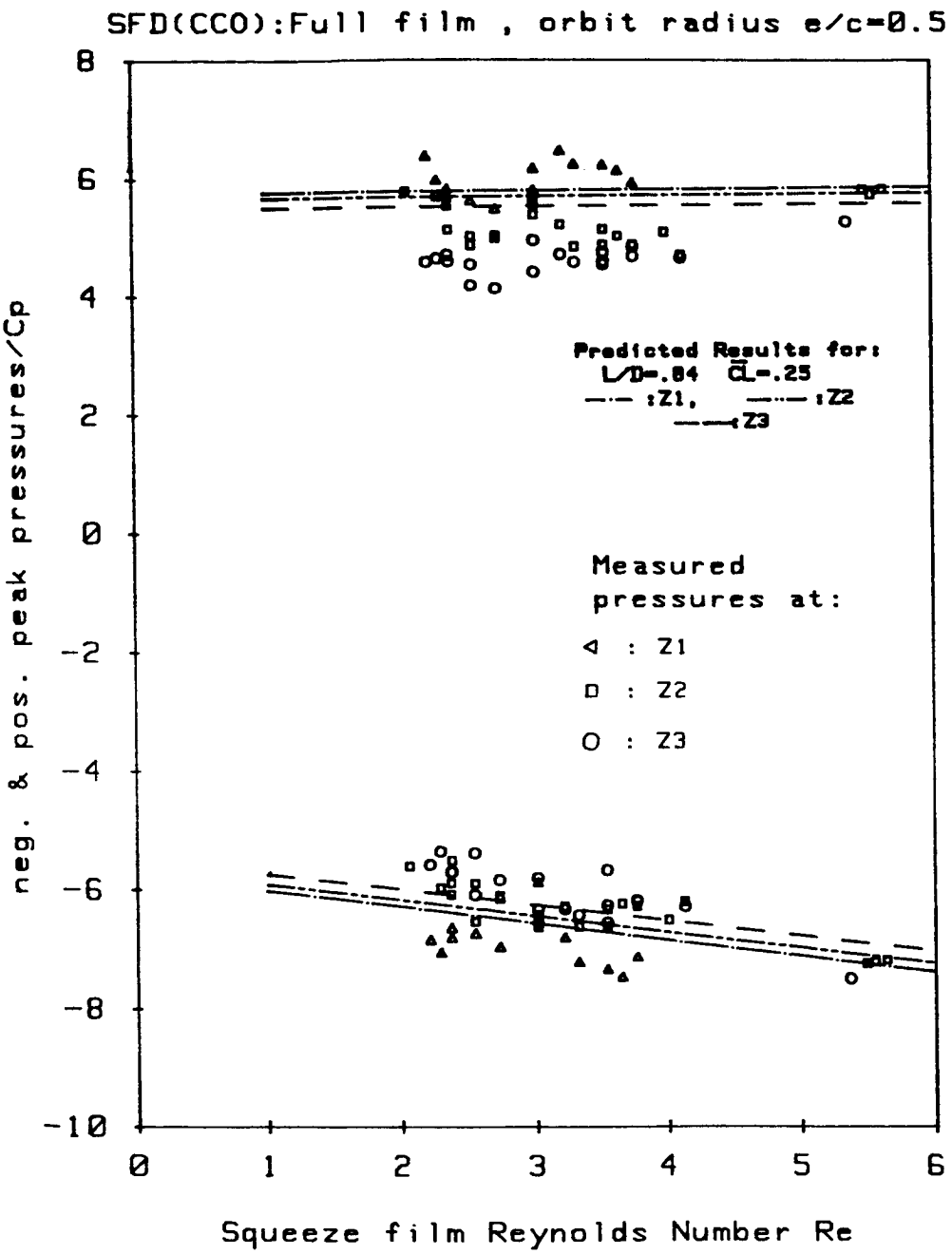

Figure 8. Dimensionless peak pressures $\bar{p}$ vs. squeeze film Reynolds. Experimenta
and predicted results.

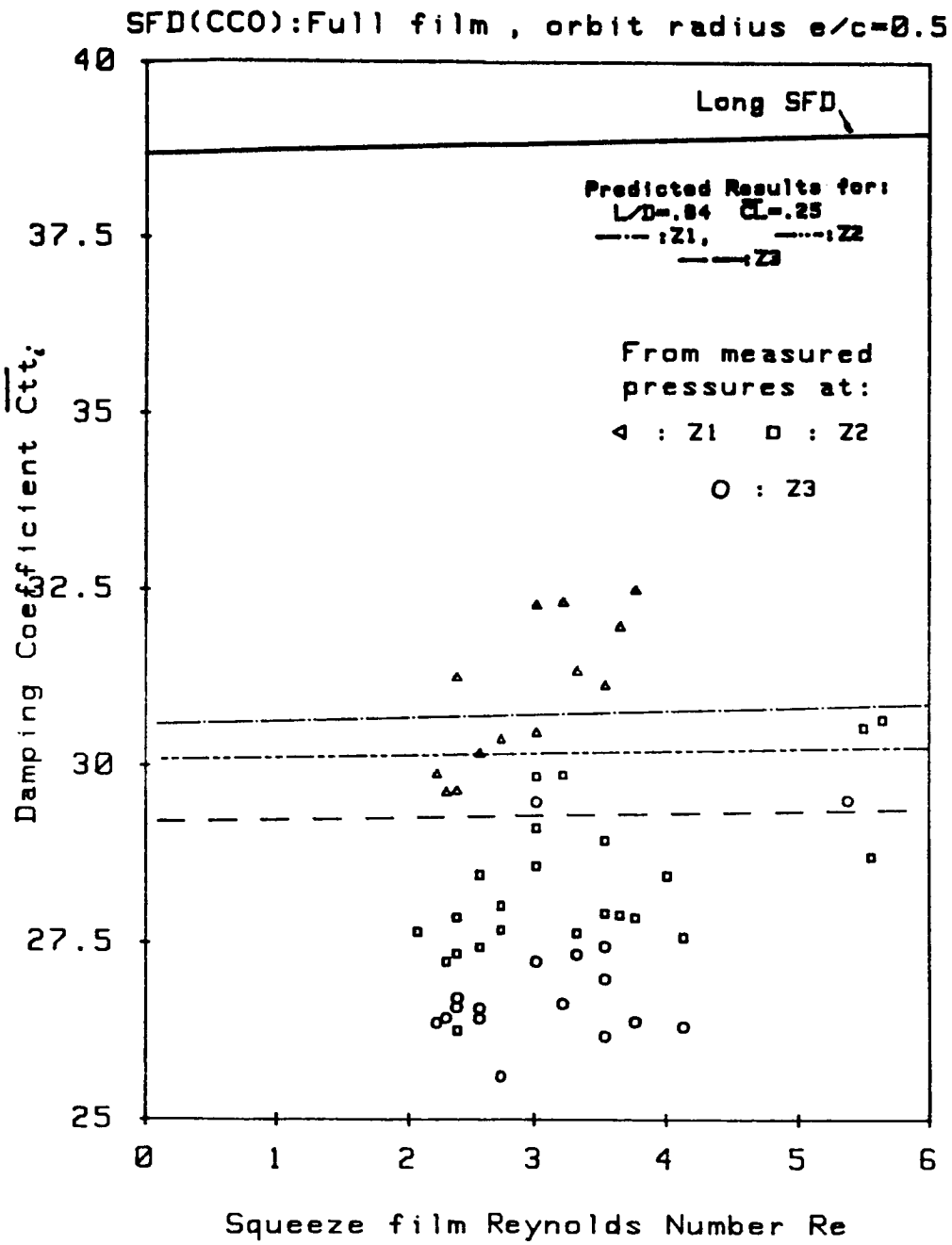

Figure 9. Dimensionless damping coefficient $\overline{Ctt}$ vs. Reynolds number calculated from measured pressures. Experimental and predicted results.

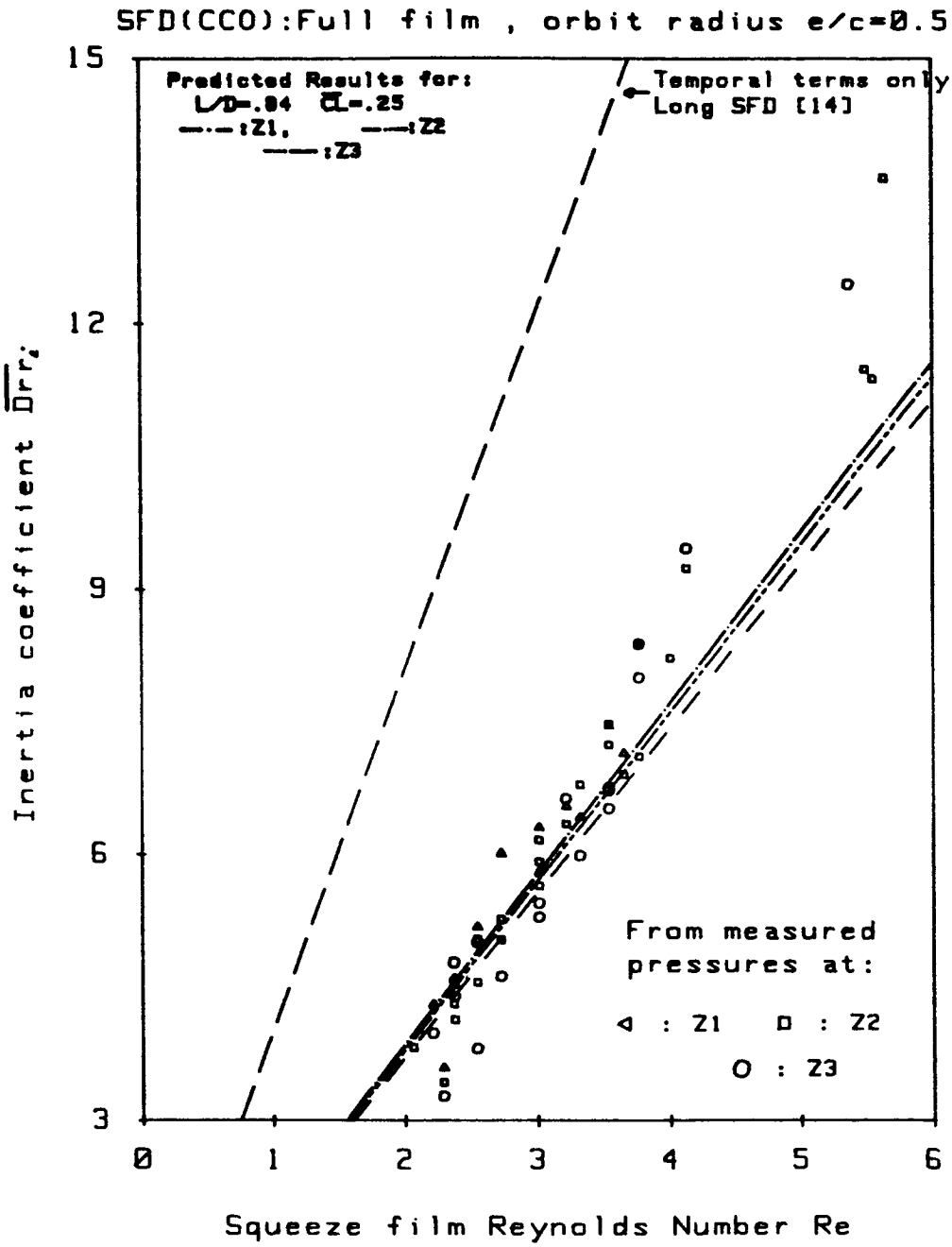

Figure 10. Dimensionless inertia coefficient $\overline{Drr}$/Re vs. Reynolds number calculated from measured pressures. Experimental and predicted results.

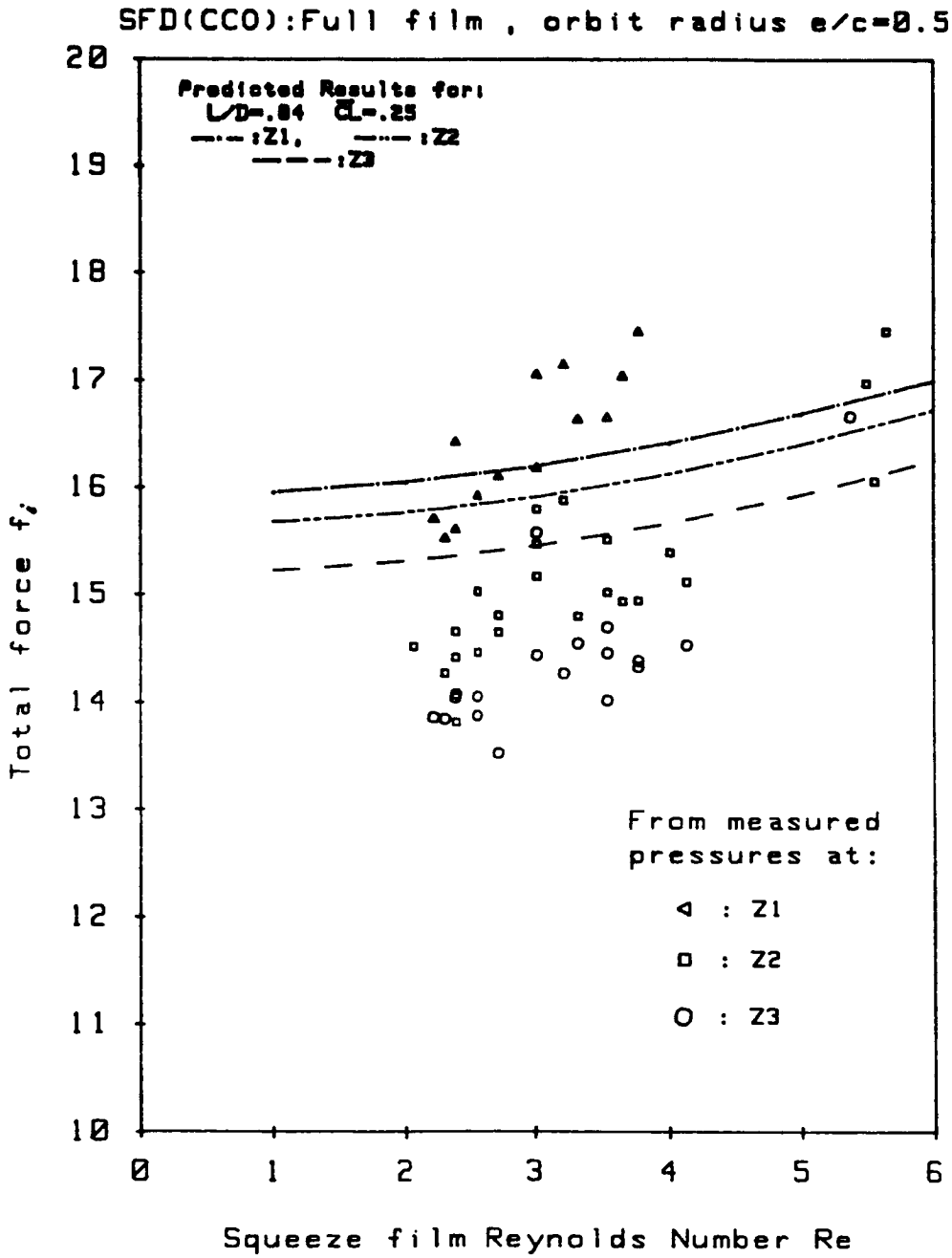

Figure 11. Dimensionless fluid film forces f vs. Reynolds number. Experimental and predicted results.

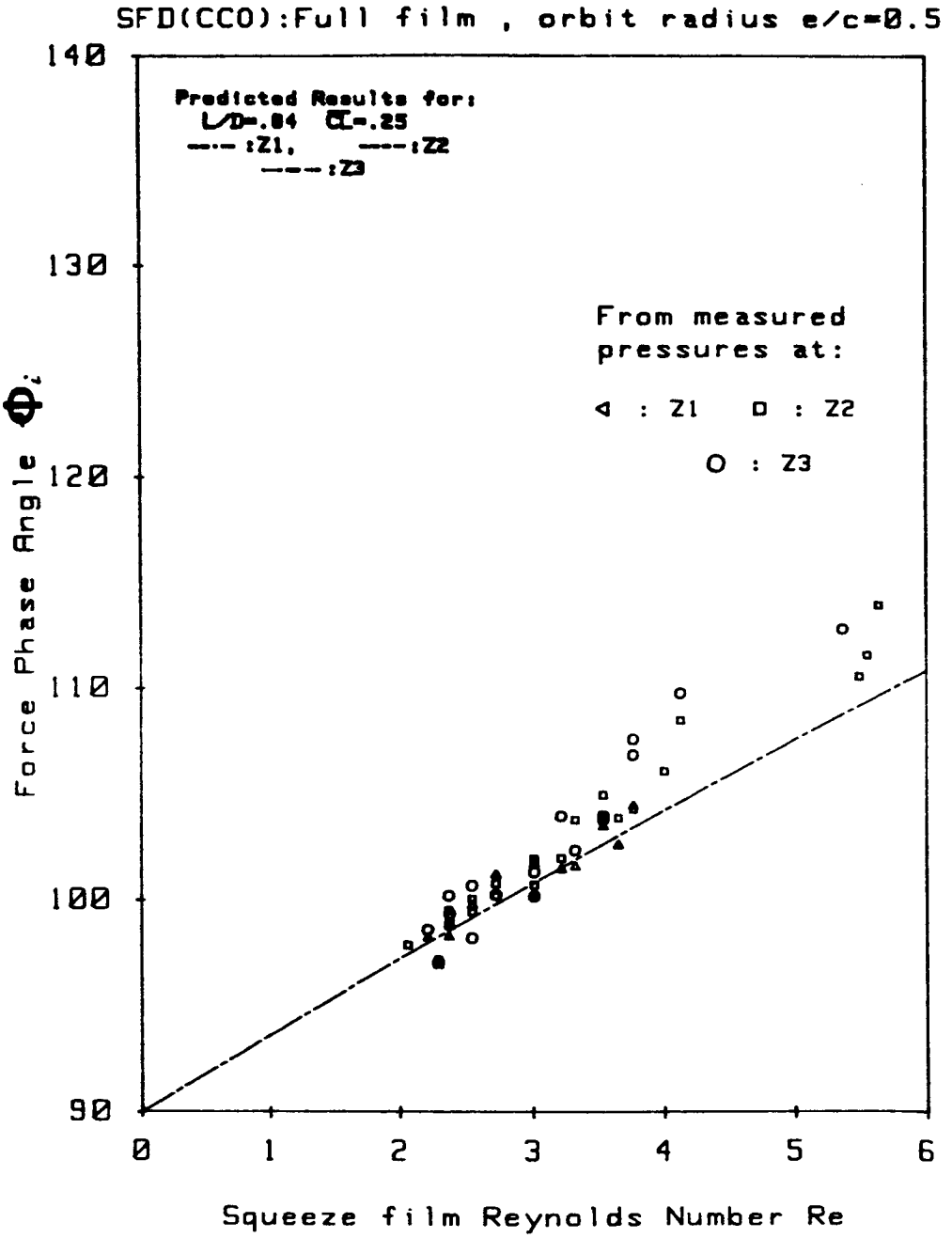

Figure 12. Force phase angle ϕ vs. squeeze film Reynolds number. Experimental and predicted results.